Plasma Flow in the Sheath and the Presheath of a Scrape-off Layer

R. Chodura

IPP 5/1

February 1985

MAX-PLANCK-INSTITUT FÜR PLASMAPHYSIK

8046 GARCHING BEI MÜNCHEN

MAX-PLANCK-INSTITUT FÜR PLASMAPHYSIK

GARCHING BEI MÜNCHEN

Plasma Flow in the Sheath and the Presheath of a Scrape-off Layer

R. Chodura

IPP 5/1 February 1985

Die nachstehende Arbeit wurde im Rahmen des Vertrages zwischen dem Max-Planck-Institut für Plasmaphysik und der Europäischen Atomgemeinschaft über die Zusammenarbeit auf dem Gebiete der Plasmaphysik durchgeführt.

TABLE OF CONTENT

Plasma Flow in the Sheath and the Presheath of a Scrape-Off Layer

PLASMA FLOW IN THE SHEATH AND THE PRESHEATH OF A SCRAPE-OFF LAYER

Roland Chodura

Max-Planck-Institut für Plasmaphysik, EURATOM

Association, D-8046 Garching, Germany

ABSTRACT

The theory of plasma-wall transition is reviewed including the effect of a magnetic field oblique to the wall leading to a double structure of the sheath. The implications of the conditions at the sheath edge on the flow in the presheath are discussed.

1. INTRODUCTION

The maintenance of a hot plasma in a fusion device is only possible if the plasma is to a large extend separated from material walls. In closed devices like tokamaks or stellarators this separation is achieved by creating the plasma within a volume of nested magnetic surfaces which are closed in themselves, so that motion along magnetic field lines will not lead to plasma loss. Nevertheless, by collisional diffusion plasma slowly leaks out of the confinement region into a loss region where magnetic field lines and at material walls, e.g. limiters or divertor plates (Fig. 1). In this loss- or scrape-off region the plasma absorbing wall establishes a pressure gradient which accelerates the plasma along the magnetic field beyond sound speed C. Thus, plasma motion in the scrape-off layer is a superposition of slow diffusion across and fast flow along magnetic field.

The scrape-off layer divides into two markedly different regions (Fig. 2):

1. A narrow region ahead of the wall with large gradients of the state variables and supersonic flow velocity, called "sheath";
2. The by far larger region upstream of the sheath with relatively weak gradients and in general subsonic flow, named "pre-sheath".

The sheath, due to its small extension, is nearly collisionfree. It is determined by the electron and ion dynamics in their electric and magnetic fields. The presheath, in general, is collision dominated. It contains the interactions among plasma particles themselves, i.e. plasma transport and relaxation processes as well as interactions between plasma and neutrals (e.g. ionization or charge

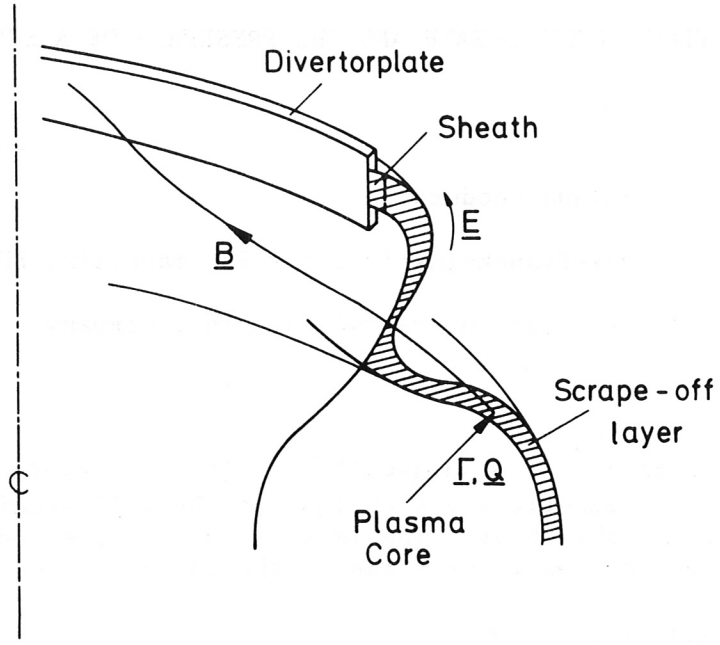

Fig. 1. Scrape-off layer in a tokamak with divertor.

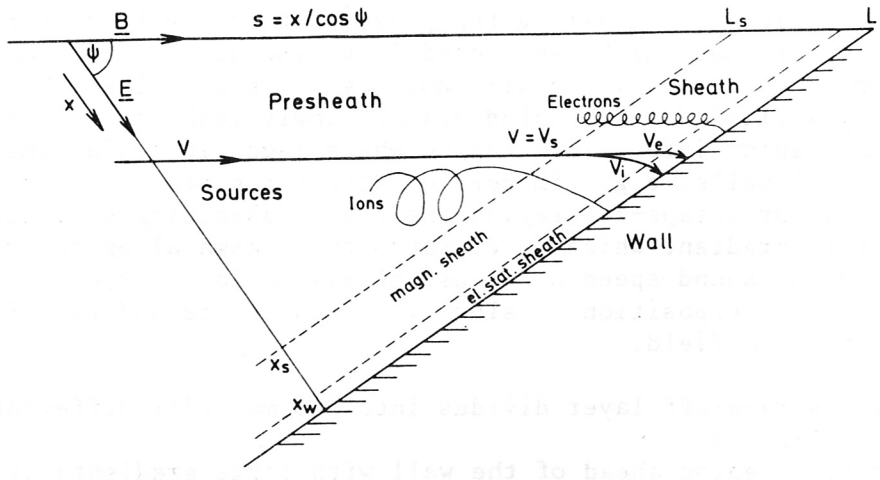

Fig. 2. Schematic view of presheath and sheath in a scrape-off layer.

exchange) which represent volume sources and sinks of plasma particle-, momentum- and energy flow.

Due to their different masses and pressure gradients ions and electrons experience different accelerations. This leads to charge separation. In order to preserve $\nabla \cdot \underline{j}=0$ of current density $\underline{j}$, an electric space charge field $\underline{E}$ is built up in the presheath and sheath region. Since gradients in the presheath are small, the electric field is relatively small as well, while it becomes large in the sheath. Accordingly, the presheath is quasineutral, i.e. ion and electron charge densities Zen_i and en_e are nearly equal there, $Zn_i \cong n_e$, where Z is the ion charge number. On the contrary, the plasma in the sheath may become non-neutral, i.e. $Zn_i > n_e$.

In an axisymmetric device such as a tokamak with toroidal limiter or divertor the electric potential field is purely poloidal while the magnetic field is mainly toroidal. So the angle between electric and magnetic field may be nearly 90° in practical cases. If the wall is a good conductor the electric field in the sheath is normal to the wall.

In the presheath the plasma flow is essentially directed along the magnetic field. The electric field, in general oblique to the magnetic field, tends to pull the flow towards its direction. Thus, in the sheath, where the electric field is fairly strong, the plasma flow is bent from magnetic field direction to the direction of the wall normal (Fig. 2).

In the following section the description of the sheath and the presheath plasma, as given by P.C. Stangeby in the previous chapter, is extended in some respects. Sections 2 and 3 present numerical models of the sheath and the presheath on the basis of the relevant length scales of the problem. Section 4 investigates the role of an oblique magnetic field on the properties of the sheath, and Section 5 discusses consequences of boundary conditions imposed by the sheath on the 1d plasma flow in the presheath.
More detailed treatments of the presheath (i.e. 2d flow, interaction with neutrals) will be given in Chapters 10, 11 and 12.

2. LENGTH SCALES OF THE SCRAPE OFF-LAYER

In order to derive a consistent model of a stationary scrape-off layer one has to consider the relevant length scales of the system. Some of them are externally given by the device, others are internally determined by the physical processes in the layer.

External length scales are:
the length L of the scrape-off layer measured along the magnetic field lines from a plane of vanishing particle and energy fluxes up to the wall or probe,

the characteristic dimension d along the magnetic field of the particle and energy fluxes fed into the scrape-off layer from the main plasma,
the characteristic dimension of the wall or probe.

Internal length scales are given by transport (i.e. diffusion, heat conduction, viscosity), relaxation (i.e. Maxwellization, temperature exchange, reistivity) of plasma particles and by their interaction with neutrals.

The extension of the scrape-off layer perpendicular to the magnetic field $l_\perp$ is determined by an "anomalous" diffusion coefficient $D_\perp$ which cannot be derived from classical transport theory,

$$D_\perp = 0.1 - 0.4 \ m^2/s$$

for tokamaks. From particle continuity one gets for $l_\perp$

$$l_\perp^2 \cong \frac{D_\perp}{v_{i\parallel}} \, l_\parallel$$

where $V_{i\parallel}$ and $l_\parallel$ are the flow velocity and characteristic length parallel $\underline{B}$ in the scrape-off layer.

Plasma transport and relaxation along the magnetic field are governed by Coulomb collisions. They are characterized by the length of mean free path for 90° deflection λ. For collisions between a test particle of velocity v and Maxwellian target particles of the same sort (i.e. electron-electron or ion-ion collisions) with mean energy $m\langle v_f^2\rangle/2 = 3\,T/2$, λ is given by

$$\lambda = \left(\frac{v}{\sqrt{3} \cdot v_t}\right)^4 \lambda_t \qquad (2.1)$$

where λ_t is the mean free path length for a test particle with energy $m\,v^2/2 = 3\,T/2$,

$$\lambda_t = \sqrt{3}\, v_t\, t_c \cong 1.5 \cdot 10^{16}\, T^2/n\,, \qquad (2.2)$$

T and n are temperature and density of the target particles respectively, $v_t = (T/m)^{1/2}$ is the thermal speed and t_c the self-collision time /1/. T stands for $k_B T$ throughout the text, where k_B is the Boltzmann constant. In equ.(2.2) T is measured in eV, all other quantities in mks-units. Electron-ion collisions have a mean free path only by a factor $1/\sqrt{2}$ shorter than that for electron-electron colllisions. λ_t is plotted in Fig. 3.

From λ_t one can derive several transport coefficients. Of special importance for the energy transport in the scrape-off layer is the electron heat conduction along the magnetic field

$$q_e = - \chi_{e\parallel} \nabla_{\parallel} T_e \qquad (2.3)$$

where q_e and T_e are electron heat flux and temperature respectively. Heat conduction $\chi_{e\parallel}$ is given by /2/

$$\chi_{e\parallel} = 2.9 \cdot 10^{-19} n_e v_{te} \lambda_t \cong 1.8 \cdot 10^3 T_e^{5/2}, \qquad (2.4)$$

T_e and ∇T_e are measured in eV and eV/m respectively, heat flux q_e in W/m^2.

Ion parallel heat conductivity $\chi_{i\parallel}$ is smaller by a factor of order square root of the mass ratio $(m_e/m_i)^{1/2}$ than $\chi_{e\parallel}$,

$$\chi_{i\parallel} = 5.1 \cdot 10^{-19} n_i v_{ti} \lambda_t \cong 75 \cdot T_i^{5/2} \qquad (2.5)$$

and therefore less important.

If a certain amount of heat flux $q_{e\parallel}$ has to be transported along B to the wall an electron temperature gradient with characteristic length $\Lambda_{e\parallel}$ will arise where

$$\Lambda_{e\parallel} = \chi_{e\parallel} T_e / q_{e\parallel} = 2.9 \cdot 10^{-19} (n_e v_{te} T_e / q_{e\parallel}) \lambda_t$$
$$\cong 1.8 \cdot 10^3 T_e^{7/2} / q_{e\parallel}. \qquad (2.6)$$

$\Lambda_{e\parallel}$ is plotted in Fig. 3 for $q_{e\parallel} = 10^8$ W/m^2.

It has to be pointed out, however, that in order equ. (2.3) to be valid electrons which contribute most to the heat flux, i.e. those with $v_q \cong 3.7\, v_{te}$, have to have a mean free path λ_q smaller than the temperature gradient length $\Lambda_{e\parallel}$. According to (2.1) the mean free path is proportional to v^4. Therefore the applicability of equ.(2.3) is restricted to rather small gradients /3/

$$\Lambda_{e\parallel} > \lambda_q = (v_q/\sqrt{3}\, v_{te})^4 \lambda_t = 21\, \lambda_t$$

or, by equ. (2.6),

$$q_{e\parallel} < 1.0 \cdot 10^{-20} n_e v_{te} T_e . \qquad (2.7)$$

For steeper gradients the heat flux at a point becomes non-local, i.e. it is no more determined by the local temperature gradient at this point but by a weighted mean of the temperature profile over a distance of about $\pm 5\, \lambda_t$ around this point /4/.

Another important length scale is defined by the relaxation of the electron velocity distribution to a nearly Maxwellian one. As will be shown in Section 4 the electron distribution ahead of the sheath is depleted at velocities $|v| > |v_c|$ where $m_e v_c^2 / 2 \cong 3\, T_e$ due to

losses to the wall. With increasing distance from the wall this loss region is filled up by collisions, i.e. the electron distribution is isotropized by electron-ion and electron-electron-collisions and Maxwellized by electron-electron collisions. Both processes have about the same length scale of

$$\Lambda_{re} = \left(\frac{v_c}{\sqrt{3}\, v_{te}}\right)^4 \lambda_t \cong 4\, \lambda_t . \tag{2.8}$$

The relaxation of different electron and ion temperatures to a common temperature during the flow to the wall occurs on a much longer length scale of about mass ratio times λ_t,

$$\Lambda_{t\ e,i} \cong \frac{m_i}{m_e}\, \lambda_t . \tag{2.9}$$

Out of the huge amount of interactions of plasma with neutrals only two important processes are presented in Fig. 3, i.e. ionization and charge exchange collisions: A neutral H atom at Frank-Condon energy of about $m_i v_o^2/2 = 4$ eV transverses a mean free path of λ_{ion} before being ionized by collisions with electrons of velocity v_e,

$$\lambda_{ion} = \frac{v_o}{n_e \langle \sigma_{ion}\, v_e \rangle} , \tag{2.10}$$

and a mean free path λ_{CX} before exchanging its charge with an H+-ion of velocity v_i,

$$\lambda_{cx} = \frac{v_o}{n_i \langle \sigma_{cx}\, v_i \rangle} . \tag{2.11}$$

Both path lengths are shown in Fig. 3 for thermal electrons and ions of temperatures T.

The shortest scale lengths in the scrape-off layer are those of the sheath. As will be shown in Section 4 the part of the sheath which is determined by the magnetic field B has a characteristic thickness perpendicular to the wall of the order of the ion gyroradius at sound speed $C = (2T/m_i)^{1/2}$. For oblique angles

$$\lambda_m \cong 4C/\omega_{ci} , \tag{2.12}$$

where ω_{ci} is the ion gyrofrequency for H^+ ions, $\omega_{ci} = eB/m_i$. The projection of d_m along $\underline{B}$, $d_m/\cos\psi$, where ψ is the angle between $\underline{B}$ and the wall normal is plotted in Fig. 3 for B = 2 T and $\psi = 85°$.

Immediately ahead of the wall extends the electrostatic Debye sheath over about 10 Debye lengths λ_D perpendicular to the wall,

$$\lambda_{es} \cong 10\, \lambda_D . \tag{2.13}$$

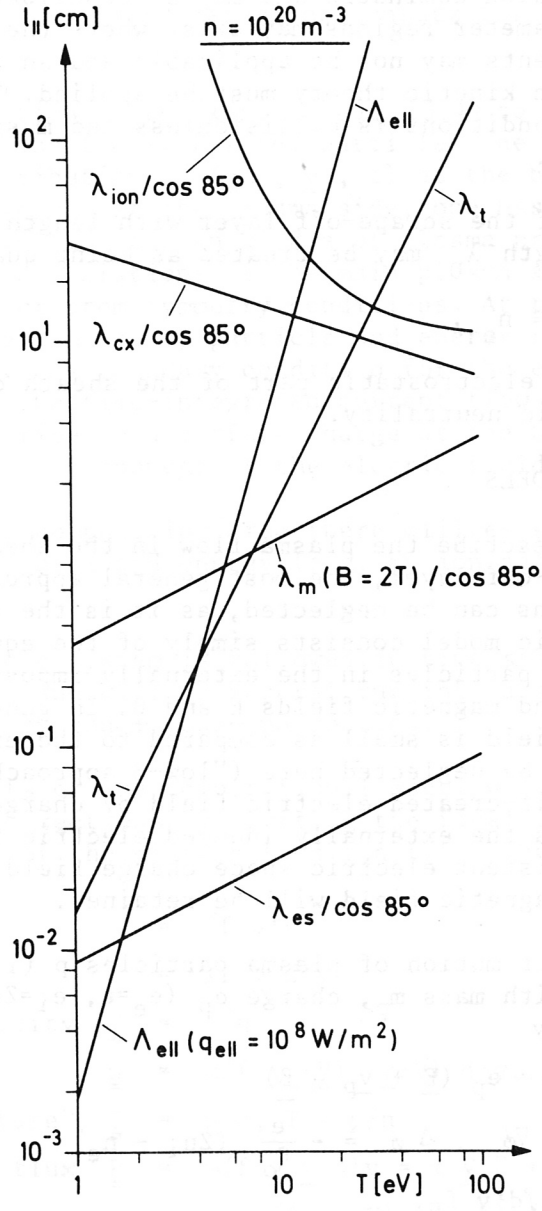

Fig. 3. Length scales $l_{\parallel}(n,T)$ along the magnetic field in the scrape-off layer (for hydrogen).

The projection of λ_{es} along B, $\lambda_{es}/\cos\psi$, is plotted in Fig. 3 again for $\psi = 85°$.

From inspection of Fig. 3 one can see that the presheath is more or less collision-dominated and may be described by a fluid model but that parameter regions may exist where the Braginskii transport coefficients may not be applicable and an improved transport theory or even kinetic theory must be applied. The sheath under nearly all conditions is collisionless and must be described by a kinetic model.

All regions of the scrape-off layer with length scales larger than the Debye length λ_D may be treated as being quasineutral, i.e.

$$Z\, n_i \cong n_e \,.$$

Thus only the electrostatic part of the sheath deviates appreciably from electric neutrality.

3. MATHEMATICAL MODELS

In order to describe the plasma flow in the sheath and presheath region of a scrape-off layer, the most general approach is a kinetic model. If collisions can be neglected, as it is the case in the sheath, this kinetic model consists simply of the equation of motion of the plasma particles in the externally imposed and self-created electric and magnetic fields $\underline{E}$ and $\underline{B}$. In general the self-created magnetic field is small as compared to the externally applied one and will be neglected here ("low-ß approach"). On the other hand, the self-created electric field by charge separation in general far exceeds the externally induced electric field. Thus only the self-consistent electric space charge field and a prescribed external magnetic field will be retained.

The equation of motion of plasma particles p (i.e. ions i and electrons e) with mass m_p, charge e_p (e_e=e, e_i=Ze) and velocity $\underline{v}_p$ is then given by

$$m_p\, \dot{\underline{v}}_p = e_p\, (\underline{E} + \underline{v}_p \times \underline{B}) \qquad (3.1)$$

where

$$\underline{E} = -\nabla\phi \quad , \quad \Delta\phi = -\frac{e}{\varepsilon_o}\,(Zn_i - n_e) \qquad (3.2)$$

$$n_p = \int d^3v\, f_p \,. \qquad (3.3)$$

$f_p(\underline{x}, \underline{v}, t)\, d^3x\, d^3v$ is the number of particles p counted in a phase volume $d^3x\, d^3v$. Equations (3.1) to (3.3) represent the collisionless "Vlasov model".

If one intends to apply the kinetic model to the larger length scales of the presheath, one has to include collisions. In the equation of motion (3.1) a term $m_p\, \dot{\underline{v}}_{p\ \mathrm{coll}}$ must be added, which

accounts for the dynamical friction and stochastic diffusion in velocity space of particle p by collisions with other plasma particles,

$$\dot{v}_{coll} = \dot{v}_{dyn.\,fr.} + \dot{v}_{diff} \quad . \tag{3.4}$$

Equ. (3.4) represents the Fokker-Planck ansatz for Coulomb collisions / 5 /.

For a solution of the kinetic eqs. (3.1) to (3.3) one has to impose boundary conditions: For the particles one has to prescribe the velocity distribution $f_p^+ (\underline{x}_b , \underline{v} , t)$ at the boundary $\underline{x}_b$ for instreaming particles. At the plasma side, one has to infer this boundary condition from the knowledge of plasma properties, for instance, by fluid calculations of the main plasma and parts of the scrape-off layer or from symmetry conditions. At the wall boundary conditions are determined by particle and energy reflexion properties of the wall. As boundary condition for the electric field it is assumed that the time-integrated current flow into and out of the system gives rise to a surface charge at the boundary which determines the normal component of the elctric field.

Within the computation area there will exist sources or sinks of particles, momentum and energy (e.g. by ionization or charge exchange).

The particle system is followed in time starting from some initial condition and will in general run into a steady state for stationary boundary conditions and sources.

The results of the computational model will be presented in the following two sections by plotting the final steady-state profiles of moments of the distribution function. The lowest order moments are

density	n	$= \int f \, d^3v$
flux	$\underline{\Gamma}$	$= \int f \, \underline{v} \, d^3v$
flow velocity	$\underline{V}$	$= \underline{\Gamma}/n$
pressure	$\underline{\underline{p}}$	$= m\int f \, (\underline{v}-\underline{V}) \, (\underline{v}-\underline{V}) \, d^3v$, $p = \frac{m}{3}\int f \, (\underline{v}-\underline{V})^2 \, d^3v$
"temperature"	$\underline{\underline{T}}$	$= \underline{\underline{p}}/n$, $T = p/n$
momentum flux	$\underline{\underline{P}}$	$= m\int f \, \underline{v} \, \underline{v} \, d^3v = m \, \underline{V} \, \underline{\Gamma} + \underline{\underline{p}}$
heat flux	$\underline{q}$	$= m/2 \int f \, (\underline{v}-\underline{V})^2 \, (\underline{v}-\underline{V}) \, d^3v$
energy flux	$\underline{Q}$	$= m/2 \int f \, v^2 \, \underline{v} \, d^3v =$
		$= [(m/2 \, V^2 + T/(\gamma-1)] \, \underline{\Gamma} + \underline{\underline{p}} \cdot \underline{V} + \underline{q}$, $\gamma = 5/3$.

($\underline{\underline{T}}$ is not a temperature in the thermodynamic sense but indicates the width of the velocity distribution.)

These moments satisfy certain conservation relations, i.e. for

particle density $\partial n/\partial t + \nabla\cdot\underline{\Gamma} = S_n$

momentum $\partial(m\underline{\Gamma})/\partial t + \nabla\cdot\underline{\underline{P}} = ne\ (\underline{E} + \underline{V}\times\underline{B}) + \underline{S}_m$

energy $\partial(nmV^2/2 + p/(\gamma-1))/\partial t + \nabla\cdot\underline{Q} = e\underline{\Gamma}\cdot\underline{E} + S_q$. (3.6)

S_n, $\underline{S}_m$ and S_q are sources of particle number density, momentum and energy.

The set of conservation equations (3.6) for ions and electrons together with equation (3.2) for the electric field, may serve as a base for a fluid description of the plasma /2/ in the scrape-off layer. To this end the third order moment must be expressable by lower order moments, as for instance in equ. (2.3). This is only possible if the mean free path of plasma particles is sufficiently smaller than the macroscopic gradient lengths of the plasma (see Section 2).

If the plasma is quasineutral, equ. (3.2) may be omitted and the electric field is implicitly determined by the quasineutrality condition

$$Zn_i = n_e \ . \tag{3.7}$$

The set of conservation equations (3.6) may serve as a base for a qualitative understanding of the plasma flow in the scrape-off layer. Assume that the flow is stationary ($\partial/\partial t = 0$) and one-dimensional ($\nabla \equiv \partial/\partial x$). If there were

no sources, $S = 0$,

no net space charge, $Z\, n_i\, e = n_e\, e = n\, e$,

no current, $Z\, e\, \underline{\Gamma}_i = e\, \underline{\Gamma}_e = \underline{\Gamma}$,

it would follow from (3.6) that

$$\begin{aligned} \underline{\Gamma}_x &= \text{const} \\ \underline{\underline{P}}_{xi} + \underline{\underline{P}}_{xe} &= \text{const} \\ \underline{Q}_{xi} + \underline{Q}_{xe} &= \text{const.} \end{aligned} \tag{3.8}$$

If furthermore there were no transport, i.e. no heat flux, $\underline{q} = 0$, and no viscosity, p isotropic, $p = nT$, then from (3.8)

$$\begin{aligned} n &= \text{const} \\ \underline{V} &= \text{const} \\ T_i + T_e &= \text{const.} \end{aligned} \tag{3.9}$$

Thus, under the assumptions made, the conservation relations would prohibit any spatial change of the fluid variables.

The actual changes of flow variables in the 1d stationary flow of the scrape-off layer thus originates from

1. sources and transport in the presheath
2. the Lorentz force $\underline{j} \times \underline{B}$, $\underline{j} = e\,(Z\underline{\Gamma}_i - \underline{\Gamma}_e)$, in the magnetic sheath
3. the electrostatic force $e\,(Zn_i - n_e)\,\underline{E}$ in the electrostatic sheath.

A two- or more dimensional flow is less restricted by conservation laws. The current component to a floating wall does not necessarily vanish as in 1d, the flow can perform circulating motions without sources etc. The features of 2d flow in the scrape-off layer will be presented in Chapter 10.

In the following two Sections the kinetic and fluid models, as described before, will be applied to investigate the 1d flow in the sheath with an oblique magnetic field and in the presheath.

4. THE SHEATH

Plasma flowing through the scrape-off layer to an absorbing wall passes two regions. In the first, plasma and energy is fed into the layer by diffusion and heat conduction from the main plasma and by ionization within the layer itself. The plasma flow becomes accelerated along the magnetic field to sonic or supersonic velocities at length scales of the sources, the transport processes and the interactions with neutrals. This region is sometimes called "presheath".

The second region, called "sheath" is directly attached to the wall. It is to a large extent determined by the electron reflexion conditions of the wall. Within the sheath plasma flow is accelerated further but in general at much smaller scale lenghts than in the presheath, i.e. at the ion gyro radius and the Debye length. Therefore, gradients of flow variables and electric field in the sheath are much larger than in the presheath. Collisions within the sheath in general can be ignored (see Fig. 3).

The structure of the sheath depends on the magnitude and orientation of the magnetic field relative to the wall. For an oblique field the sheath exhibits a double structure of quasineutral flow at the ion gyro scale under the combined action of electric and magnetic forces followed by a region of non-neutral flow at the Debye length scale where the electric force dominates. Without or with wall-perpendicular magnetic field the sheath consists only of the electric Debye part. This case has been discussed in the preceding chapter by P.C. Stangeby. It will be used as a starting point and reference case for the more general case of an oblique magnetic field.

a) Sheath without or with perpendicular magnetic field (Debye sheath)

We assume an infinitely extended, plane wall at floating potential ϕ_w. The plasma flow through the sheath is then one-dimensional and directed along the wall-normal x ($\psi = 0$ in Fig.2). The wall is assumed to absorb ions totally and electrons to a fraction $1-\gamma_{re}$. The reemitted electron fraction γ_{re} starts with zero energy from the wall. Let us further assume that the flow in the sheath is collisionless. The stationary distribution function f_p of ions and electrons at any point x in the sheath is then determined by the distribution function of instreaming particles at the upstream sheath edge x_s, by the reflexion condition at the wall at $x = x_w$ and by the potential $\phi(x)$.

Electrons entering the sheath at x_s with potential $\phi_s = \phi(x_s)$ may have a Maxwellian distribution

$$f_e^+(x_s, \underline{v}) = f_{es}^M \quad \text{for } v_x > 0$$

$$\text{with} \quad f_{es}^M = n_{es}^M \left[m_e/(2\pi\, T_{es})\right]^{3/2} \exp\left(-\tfrac{1}{2}\, m_e v^2/T_{es}\right). \qquad (4.1)$$

The distribution for $v_x < 0$ is determined by the reflexion of electrons by the negative sheath potential and by the wall: All electrons entering the sheath with energy $m_e v_x^2/2 < e(\phi_s-\phi_w)$ are reflected in the sheath, electrons with $m_e v_x^2/2 \geq e(\phi_s-\phi_w)$ are either absorbed or inelastically reflected at the wall. Thus, the absorbing wall leads to an electron velocity distribution with a loss region:

$$f_e(x,\underline{v}) = \begin{cases} f_{es}^M \exp\left[e(\phi-\phi_s)/T_{es}\right] + f_{re}\,, & v_x \geq v_c \\ 0\,, & v_x < v_c \end{cases} \qquad (4.2)$$

where $v_c = -\left[2e(\phi-\phi_w)/m_e\right]^{1/2}$ is the velocity of an electron starting at the wall with $v = 0$, f_{re} is the number of electrons at x_c having been reemitted from the wall.

The distribution function of ions at the sheath edge x_s depends on the conditions in the presheath. Due to the acceleration in the presheath, their distribution is shifted to a positive mean velocity V_s and since no ions are reflected in the sheath or at the wall, f_{is} vanishes for $v_x < 0$.

Figure 4 shows a schematic picture of the changes of ion and electron distributions within the sheath. The negative potential accelerates ions towards the wall, whereas it reflects electrons to a great extent. Therefore, approaching the wall f_e decreases with the Boltzmann factor $\exp\left[e(\phi-\phi_s)/T_{es}\right]$ of equ. (4.2) and the loss region at negative velocities grows until at the wall $x = x_w$ only electrons with $v_x \geq 0$ are present, since the wall was assumed to be totally energy absorbing.

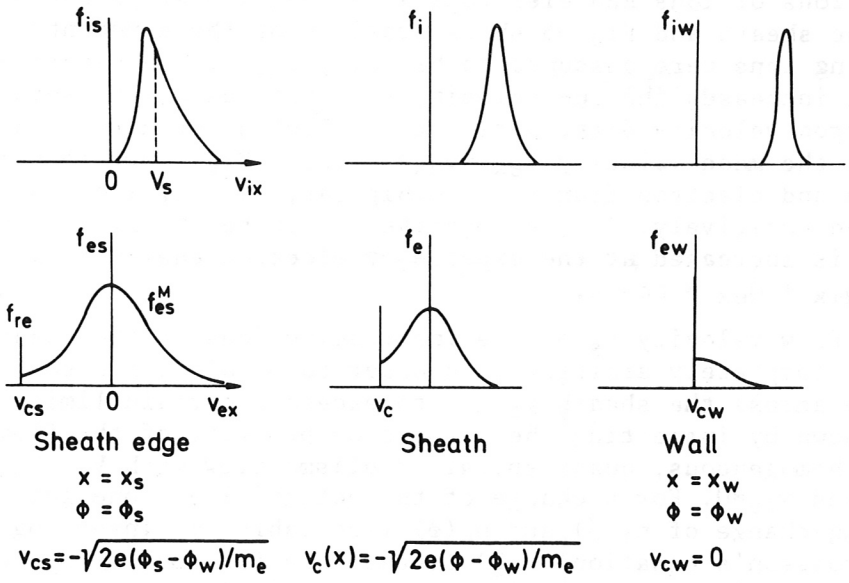

Fig. 4. Schematic velocity distributions of ions and electrons in a sheath without or with perpendicular magnetic field. Electrons are partly reemitted from the wall without initial energy.

Moment	Ions	Electrons
n	Γ_i / V_{ix}	$\frac{1}{2} n_{es}^M [1-\mathrm{erf}(\frac{v_c}{\sqrt{2}\, v_{tes}})] \exp[e(\phi-\phi_s)/T_{es}]$ $+ \frac{\gamma_{re}}{1-\gamma_{re}} \lvert\Gamma_e\rvert / \lvert v_c \rvert$
V_x	$\sqrt{V_s^2 - 2 Z e(\phi - \phi_s)/m_i}$	Γ_e / n_e
Γ_x	Γ_i	$\Gamma_e = \frac{1}{\sqrt{2\pi}} (1-\gamma_{re}) n_{es}^M v_{tes} \exp[(\phi_w - \phi_s)/T_{es}]$
T_{xx}	0	without reflected electrons $T_{es} + m_e V_{ex} (v_c - V_{ex})$
Q_x	$[m_i V_s^2/2 - Ze(\phi-\phi_s)] \Gamma_i$	$[\frac{2}{1-\gamma_{re}} T_{es} + e(\phi-\phi_w)] \Gamma_e$

Table 1: Moments of ions and electrons in a sheath without or with perpendicular magnetic field. At $x = x_s$: $V_{ix}=V_s$, $T_i=0$, $T_e=T_{es}$, $v_{te}=v_{tes}=(T_{es}/m_e)^{1/2}$. A fraction γ_{re} of wall-incident electrons is re-emitted with zero energy.

Table 1 gives the appropriate low-order moments of the velocity distributions of ions and electrons as a function of potential ϕ within the sheath and Fig. 5 shows profiles of these moments over x. Instreaming ions were asssumed to be cold, $T_{is}=0$. The negative sheath potential increases the ion velocity V_{ix}, but, as may be seen from the electron velocity distribution f_e of Fig. 4, even to a larger extent also the mean velocity $V_{ex}=\langle v_{ex}\rangle$, $V_{ex} > V_{ix}$. Correspondingly, since ion and electron flux Γ_x is ambipolar, $n_i > n_e$, i.e. the sheath is charged positively. In the negative sheath potential ion energy flux Q_{ix} is increased at the expense of electron energy flux Q_{ex}, so that $Q_{ix} + Q_{ex} = \text{const}$.

The flow velocity V_s of the instreaming ions at the sheath edge x_s is not completely arbitrary. In order to obtain a monotonic potential drop across the sheath V_s has to exceed a certain limit: This can be shown by inspecting the dispersion property of the flow at x_s. Assume a homogeneous, quasineutral 1d plasma flow with $V_x = V_s$, $T_{is}=0$, $T_e=T_{es}$, and $\gamma_{re}=0$. For a change of the potential ϕ one gets a corresponding change of $n_i(\phi)$ and $n_e(\phi)$ (see Table 1). Inserting n_i and n_e into Poisson's equation (3.2) linearizing for small $\phi-\phi_s$ and assuming $\phi-\phi_s \propto \exp(ikx)$ one gets a dispersion relation

$$k^2 \lambda_D^2 = (C_s^2 - V_s^2)/V_s^2 \tag{4.3}$$

as shown in Fig. 6a. $C_s=(ZT_{es}/m_i)^{1/2}$ is the isothermal sound speed at x_s for $T_{is}=0$, λ_D the Debye length. Thus a non-oscillating monotonic change of the potential, i.e. $k^2 < 0$, can only be obtained if

$$V_s \geq C_s \tag{4.4}$$

This inequality is called the Bohm condition /7,8/. It represents a condition for monotonic potential change at the Debye length scale in a 1d plasma flow without sources for cold ions. If ions have a finite thermal spread, the Bohm condition may be generalized to /9/

$$\langle v_{ix}^{-2} \rangle = \frac{1}{n_{is}} \int d^3v_i \, f_{is}/v_{ix}^2 \leq m_i/(ZT_{es}). \tag{4.4'}$$

The expressions for ion and electron fluxes Γ_{ix} and Γ_{ex} of Table 1 may be used to determine the potential drop across the sheath: From the condition of quasineutrality at x_s, $n_{es} \cong n_{es}^M \cong n_{is}$, and of vanishing net current $Ze\Gamma_i - e\Gamma_e = 0$ one gets the potential drop /6/

$$e(\phi_w - \phi_s) \cong \ln \frac{\sqrt{2\pi}\, V_s}{(1-\gamma_{re})v_{tes}} . \tag{4.5}$$

For $\gamma_{re} = 0$, $T_{is} = 0$, $V_s = C_s$ and H^+ ions $e(\phi_w-\phi_s)/T_{es} = -2.84$.

Inserting n_i and n_e from Table 1 into Poisson's equation (2.3), one gets the potential profile $\phi(x)$ of the Debye sheath. As may be seen from Fig. 5, this profile has an extension of about $\lambda_{es} \cong 10\,\lambda_D$.

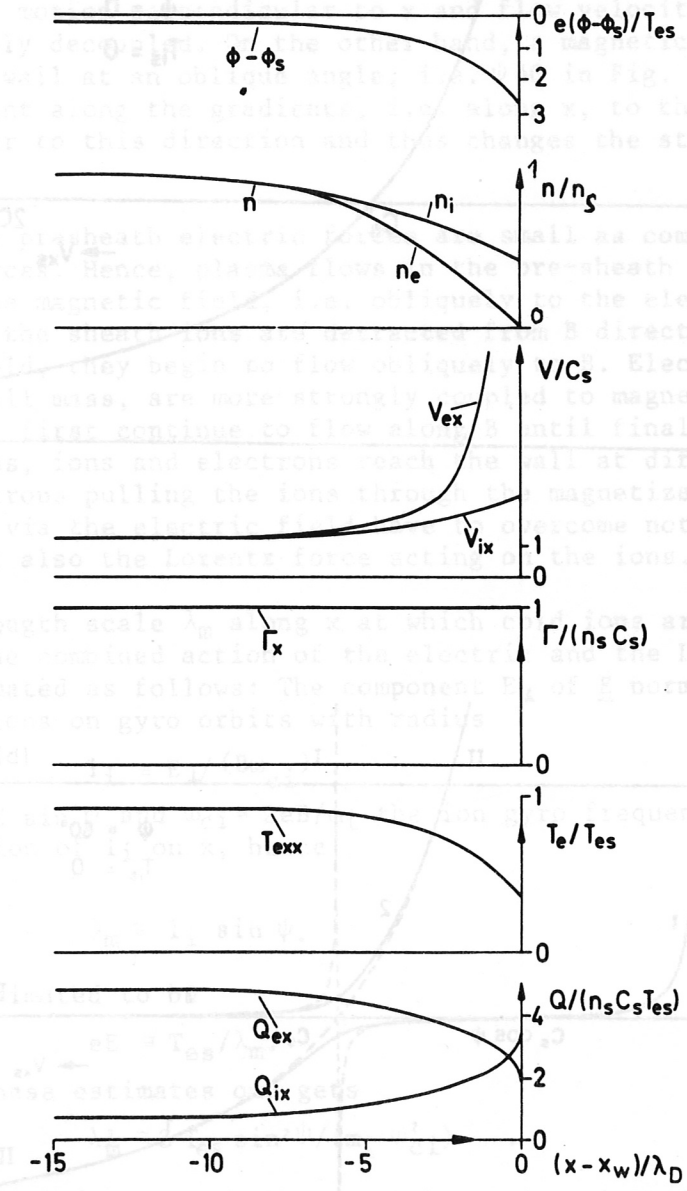

Fig. 5. Potential and flow variables (density n, mean velocity V, flux Γ, "temperature" T, energy flux Q) within the sheath for $\psi = 0$, $T_{is} = 0$, $\gamma_{re} = 0$, $m_i/m_e = 1836$.

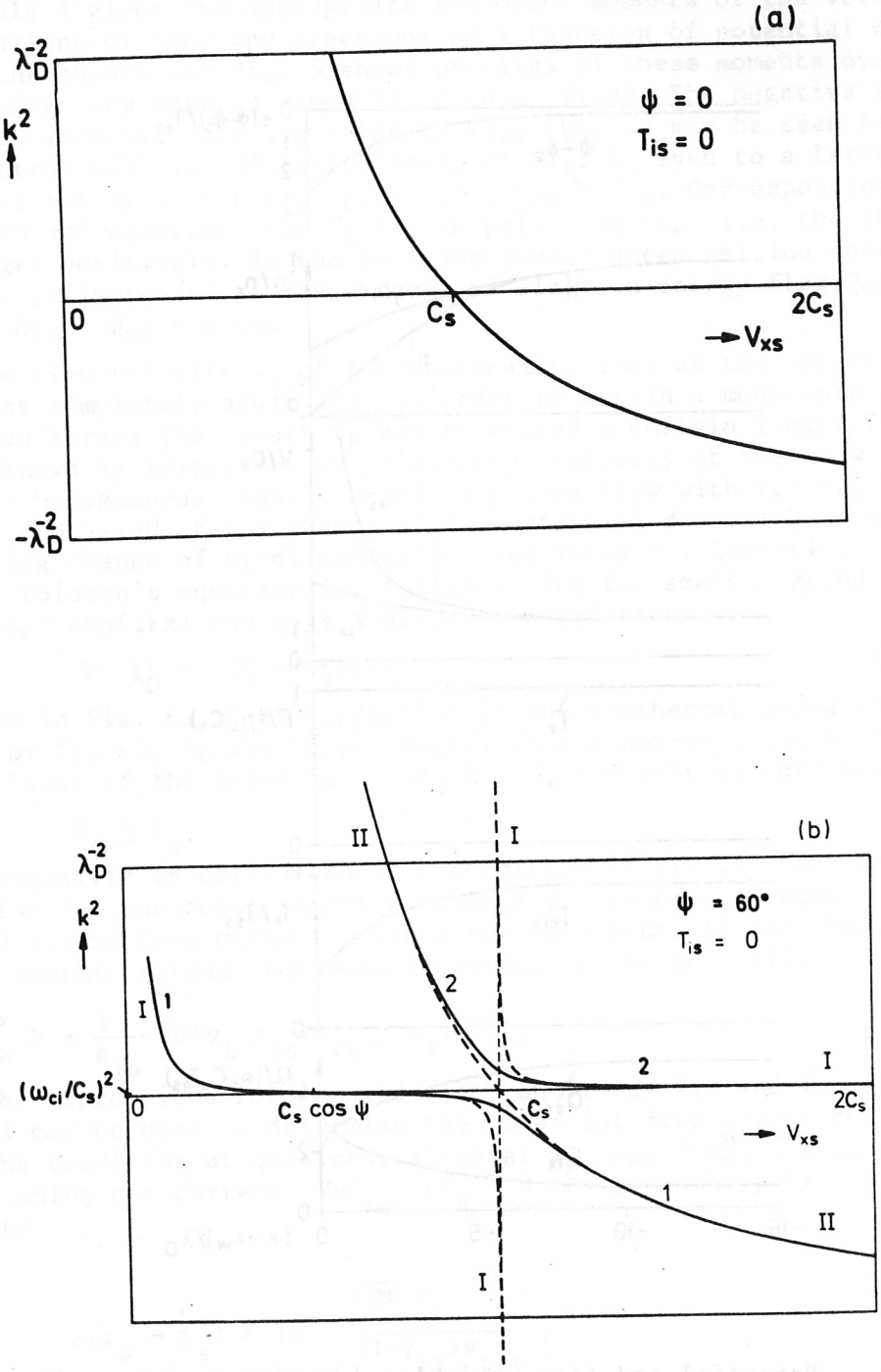

Fig. 6. Dispersion relation k^2 (V_{xs}) for cold ions
a) B = 0 or $\psi = 0$, b) $B \neq 0$, $\psi \neq 0$.

b) Sheath with oblique magnetic field

A magnetic field $\underline{B}$ perpendicular to the wall and thus parallel to the electric field $\underline{E}$ does not change the plasma flow in the sheath. Gyro motion perpendicular to x and flow velocity along x are completely decoupled. On the other hand, a magnetic field intersecting the wall at an oblique angle, i.e. $\psi \neq 0$ in Fig. 2, couples the flow component along the gradients, i.e. along x, to the components perpendicular to this direction and thus changes the structure of the sheath.

In the presheath electric forces are small as compared to magnetic forces. Hence, plasma flows in the pre-sheath nearly parallel to the magnetic field, i.e. obliquely to the electric field along x. In the sheath ions are detracted from B direction by the electric field, they begin to flow obliquely to B. Electrons, due to their small mass, are more strongly coupled to magnetic field lines and at first continue to flow along B until finally they too deviate. Thus, ions and electrons reach the wall at different flow paths. Electrons pulling the ions through the magnetized sheath to the wall via the electric field have to overcome not only the inertial but also the Lorentz force acting on the ions.

The length scale λ_m along x at which cold ions are accelerated under the combined action of the electric and the Lorentz force can be estimated as follows: The component $E_\perp$ of $\underline{E}$ normal to $\underline{B}$ forces the ions on gyro orbits with radius

$$l_i \cong E_\perp / (B\omega_{ci})$$

where $E_\perp = E \sin\psi$ and $\omega_{ci} = ZeB/m_i$ the ion gyro frequency. λ_m is the projection of l_i on x, hence

$$\lambda_m \cong l_i \sin\psi .$$

E may be estimated to be

$$eE \cong T_{es}/\lambda_m .$$

Combining these estimates one gets

$$\lambda_m^2 \cong Z\, T_{es} \sin^2\psi / (m_i\, \omega_{ci}^2) .$$

Thus, the magnetic part of the sheath has a length scale of the ion gyro radius at the ion acoustic speed $C_s = (ZT_{es}/m_i)^{1/2}$.

Further downstream in the sheath again the electrostatic Debye sheath develops. The sheath in an oblique magnetic field thus exhibits a characteristic double structure of scales λ_m and λ_{es} respectively. Since in general

$$\lambda_m >> \lambda_{es}$$

the magnetic part of the sheath is quasineutral, while the electrostatic part is non-neutral. Figure 7 shows this double structure of

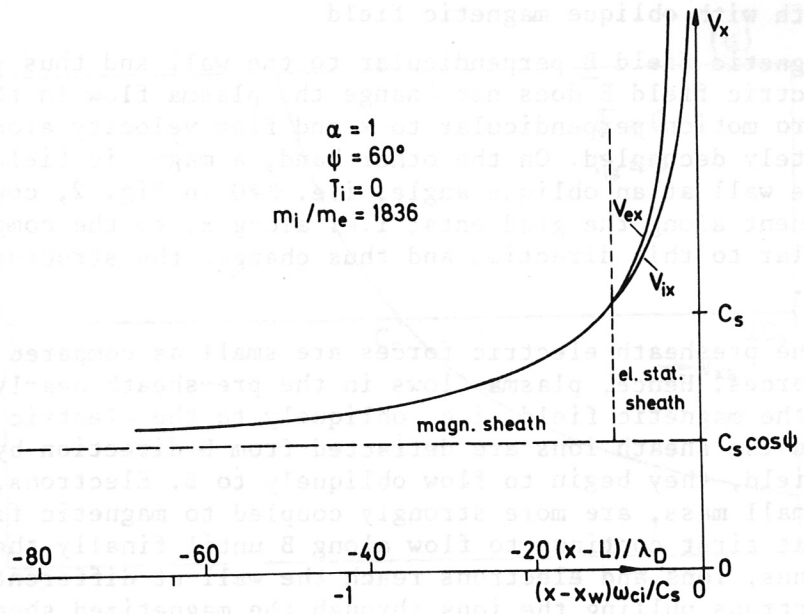

Fig. 7. Velocity profile $V_x(x)$ in a sheath with oblique magnetic field.

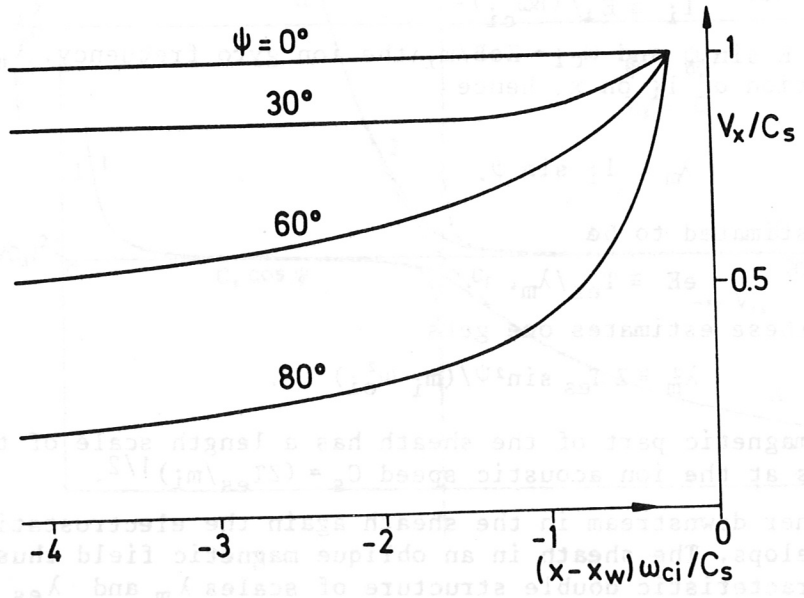

Fig. 8. Velocity profiles $V_x(x)$ in the magnetic part of the sheath.

the sheath for the x-component of flow velocity V_x of ions and electrons /10/.

As in the case of perpendicular magnetic field, the ion flow velocity at sheath entrance has to exceed a certain limit to make a monotonic potential drop possible /10/. This can again be shown by the dispersion property of the flow at x_s. A homogeneous plasma flow along the magnetic field with velocity $|\underline{V}| = V_s$ can be changed by a small disturbance $\phi-\phi_s \propto \exp(ikx)$ only for k-values which obey a dispersion relation $k^2(V_{xs})$ as shown in Fig. 6b. For each value of V_{xs} two values 1 and 2 of k^2 are possible. Curve 2 is always positive corresponding to purely oscillatory modes. Curve 2 can assume negative values $k^2 < 0$ only for

$$V_{xs} \geqq C_s \cos\psi \tag{4.6}$$

or

$$V_s \geqq C_s .$$

Thus for an exponential variation of $\phi-\phi_s$ according to mode 1 (possibly superposed by oscillations of mode 2) the flow velocity V_s along B at the sheath edge must exceed the sound speed C_s irrespective of field angle ψ. Condition (4.6) is the generalization of the Bohm condition (4.4). For $T_{is} \neq 0$ this condition is /11/

$$\langle v_{i\parallel}^{-2} \rangle = \frac{1}{n_{is}} \int d^3v_i f_{is}/v_{i\parallel}^2 \leq m_i/(ZT_{es}) \text{ with } v_{\parallel} = (\underline{v} \cdot \underline{B})/B . \tag{4.6'}$$

For $V_{xs} > C_s \cos\psi$ the decay length k^{-1} of the potential is of the order C_s/ω_{ci} and decreases with increasing V_{xs}. At

$$V_{xs} \cong C_s \tag{4.7}$$

a qualitative change in the dispersion property occurs: Curve 1 departs from the asymptotic mode I (which is a quasineutral electrostatic ion cyclotron mode) and approaches the asymptotic mode II (which is a non-neutral ion acoustic mode). The decay length k^{-1} decreases to a value of the order of the Debye length. Thus condition (4.7) represents the Bohm condition for the onset of the electrostatic part of the sheath in case of an oblique magnetic field.

The dispersion properties of Fig. 6b may be recognized in the profiles of the flow velocity V_x in Fig. 7: In the magnetic sheath the flow is quasineutral, i.e. $V_{ix}=V_{ex} = V_x$. V_x increases from $C_s \cos\psi$ to C_s on a length scale

$$\lambda_m \cong C_s/\omega_{ci} . \tag{4.8}$$

The further growth of V_x at $V_x > C_s$ takes place on the Debye length scale λ_D and the flow becomes non-neutral, i.e. $V_{ix} \neq V_{ex}$.

The profiles of V_x in the magnetic sheath for different angles ψ are shown in Fig. 8. As may be seen, the characteristic thickness of the magnetic sheath is $0 \ldots 4\ C_s/\omega_{ci}$.

The double structure of the sheath may also be recognized in the potential profiles $\phi(x)$, Fig. 9, for different angles ψ /10/. It may be

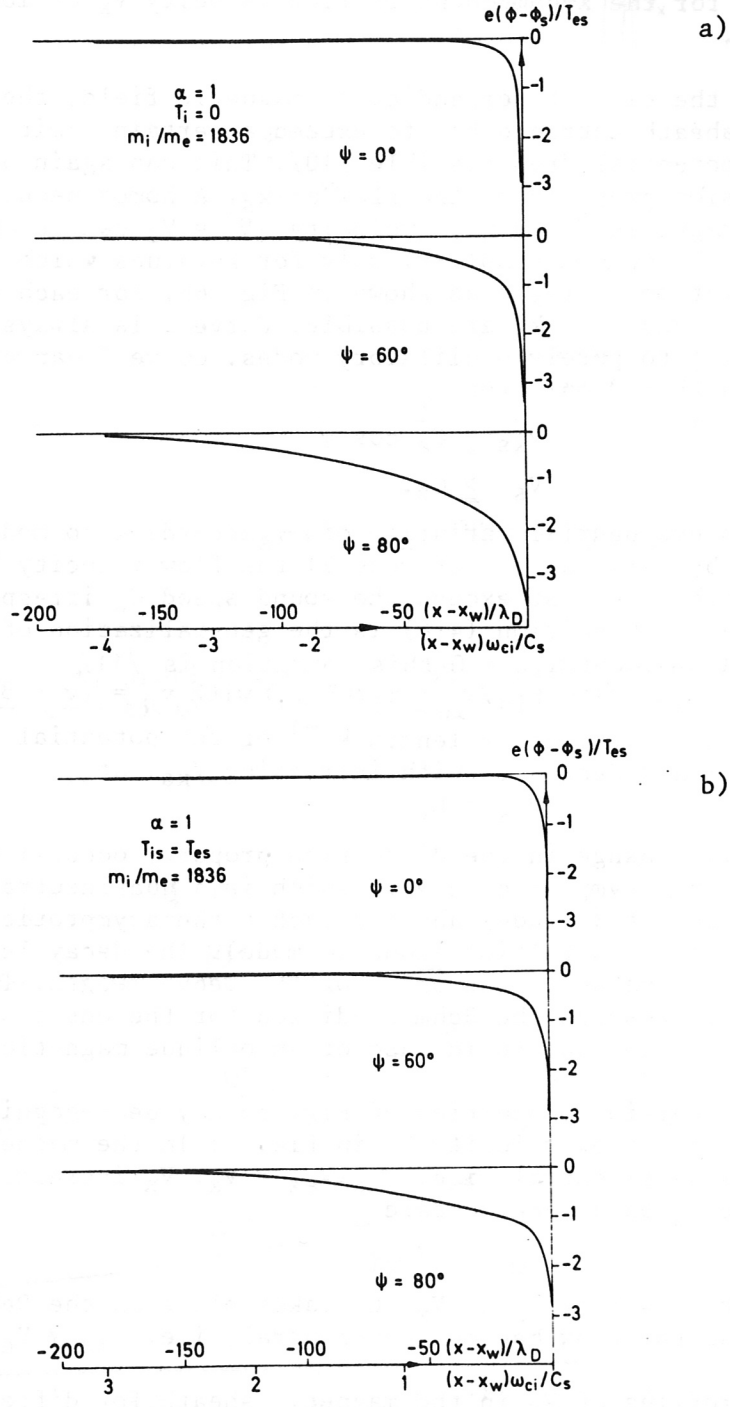

Fig. 9. Potential profiles in the sheath for different angles ψ of the magnetic field, $\gamma_{re} = 0$; a) $T_{is} = 0$, b) $T_{is} = T_{es}$.

noticed that the relative portion of potential drop in the magnetic and electrostatic part of the sheath strongly depends on ψ : The potential drop in the magnetic part of the sheath increases and the potential drop in the electrostatic sheath decreases with ψ until for $\psi \to 90°$ the whole potential drop occurs in the magnetic part and the electrostatic part of the sheath completely disappears. The reason for this behaviour is, that for increasing field angles it becomes more difficult for the ions to reach the necessary velocity V_x of equ. (4.7) for the onset of the electrostatic sheath.

Figure 10 shows the dependence of total potential drop $\phi_s - \phi_w$ across the sheath (magnetic and electrostatic) on field angle and electron reflexion coefficient γ_{re}. The curves $\gamma_{re} = 0$ correspond to the potential profiles of Fig. 9.

As may be noticed the dependence of the sheath potential $\phi_s - \phi_w$ on the angle ψ is amazingly small. This can be explained as follows: The function of the sheath potential is to adapt the electron flux component perpendicular to the wall Γ_{ex} to the ion flux component $Z\,\Gamma_{ix}$ by electron reflexion. For an ion flow velocity V_s at the sheath edge the ion flux component is $\Gamma_{ix} = n_s V_s \cos\psi$. Electrons in the magnetic sheath are magnetized i.e. their velocity distribution is rotationally symmetric around the direction of the magnetic field. If the magnetic field would be so strong that their gyroradius $l_e \ll \lambda_D$, then they would be magnetized in the electrostatic sheath either and their velocity distribution in the whole sheath would be the same as that of Fig. 4 provided that the x-direction in Fig. 4 is replaced by the direction of the magnetic field, i.e. v_{ex} changed to $v_{e\parallel}$. In particular, the electron flux would be

$$\Gamma_{ex} \cong \frac{1-\gamma_{re}}{\sqrt{2\pi}}\, n_s\, v_{tes}\, \exp[e(\phi_w - \phi_s)]\, \cos\psi,$$

Equating Γ_{ex} to $Z\,\Gamma_{ix}$ results in the same expression (4.5) for the sheath potential with oblique magnetic field as in the perpendicular case $\psi = 0$. For finite electron gyroradius l_e the velocity distribution of electrons in the sheath is changed by the more complicated absorbtion conditions at the wall. The boundary of the loss region is no longer a straight line $v_{e\parallel} = v_c$ but lies somewhere in the region $v_e^2 > v_c^2$ (for the special case $\psi = 90°$ this loss region was determined analytically in /12/, in the particle simulation model described in Section 3 it is incorporated by the reflexion condition at the wall).

For decreasing magnetic field strength, i.e. increasing electron gyroradius l_e electrons would reach the wall more easily, so the electron repelling sheath potential increases. This is shown in Fig. 11. As may be seen, for decreasing values of l_e/λ_D the sheath potential approaches the value of $\psi = 0$, i.e. $\phi_w\ (\alpha \to \infty) = \phi_w\ (\psi = 0)$.

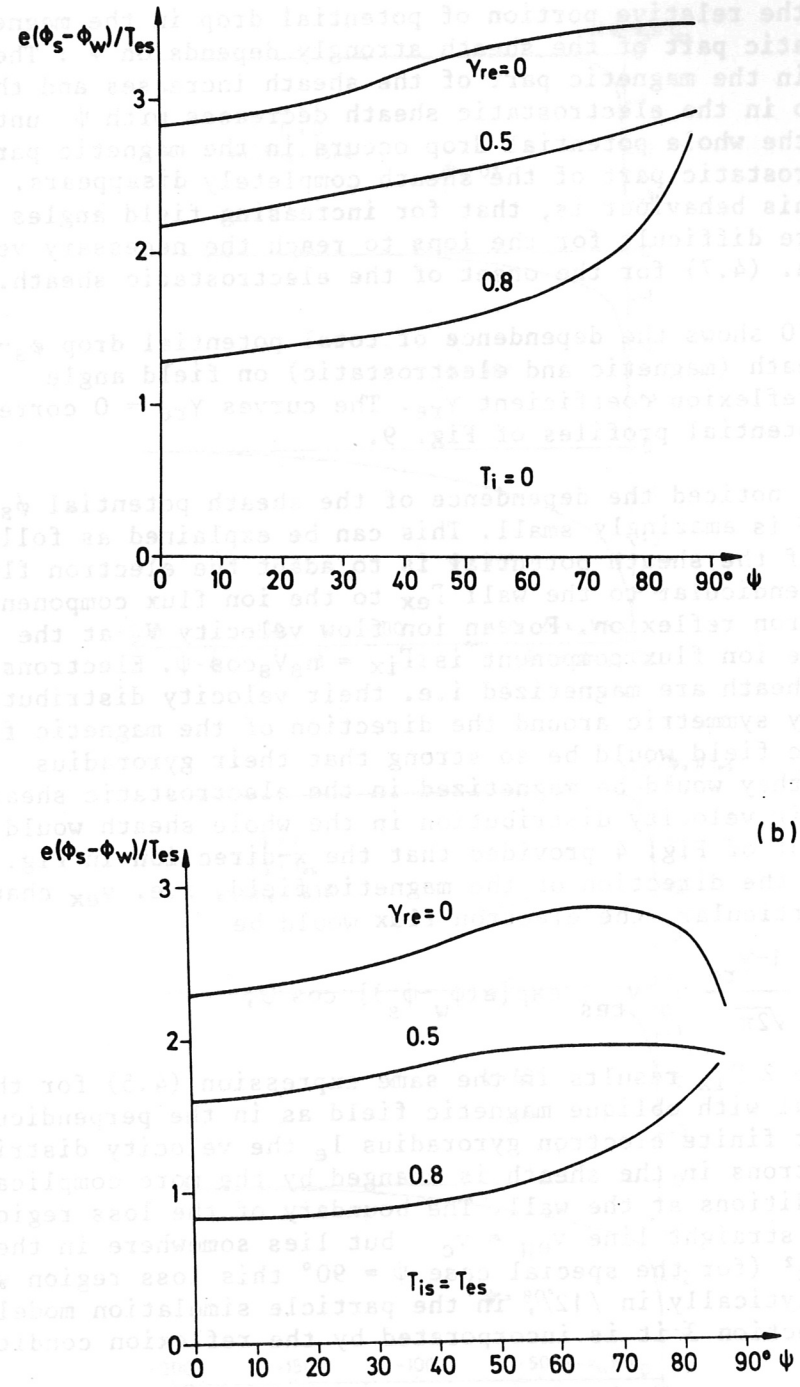

Fig. 10. Potential drop across the sheath for different angles ψ and secondary electron emission coefficients γ_{re}; a) $T_{is} = 0$, b) $T_{is} = T_{es}$.

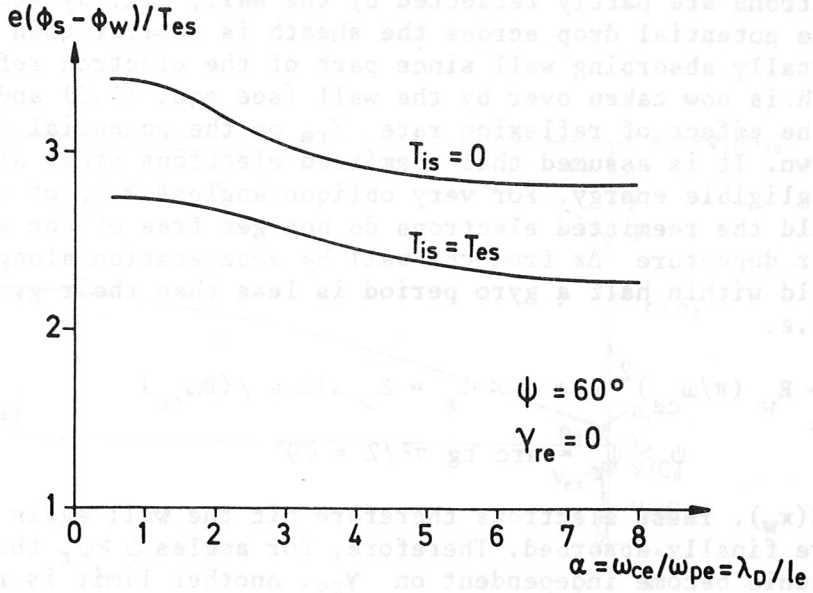

Fig. 11. Potential drop across the sheath for different magnetic field strengths. $\alpha = \omega_{ce}/\omega_{pe}$, $\psi = 60°$, $\gamma_{re} = 0$.

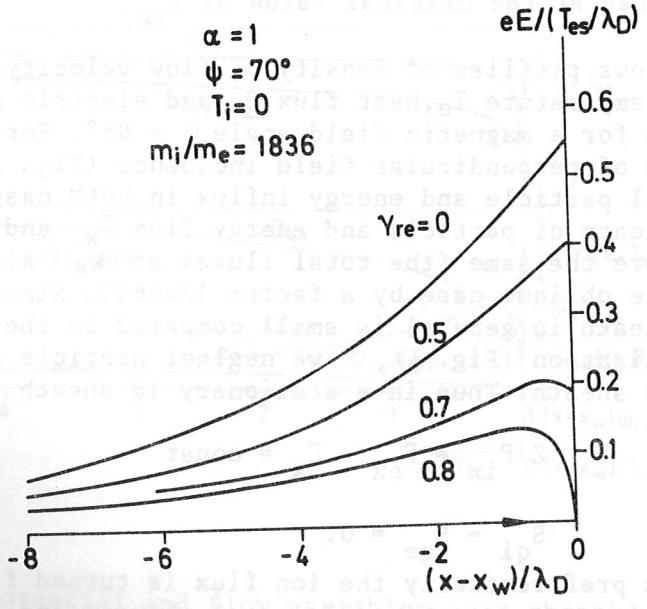

Fig. 12. Electric field near the wall for different values of secondary emission coefficient γ_{re}.

If electrons are partly reflected by the wall, e.g. by secondary emission, the potential drop across the sheath is smaller than in the case of a totally absorbing wall since part of the electron reflexion in the sheath is now taken over by the wall (see equ. (4.5) and /13/). In Fig. 10 the effect of reflexion rate γ_{re} on the potential drop $\phi_s - \phi_w$ is shown. It is assumed that reemitted electrons start at the wall with negligible energy. For very oblique angles $\psi > \psi_r$ of the magnetic field the reemitted electrons do not get free of the wall, because their departure Δx from the wall by acceleration along the magnetic field within half a gyro period is less than their gyroradius l_e, i.e.

$$\Delta x = \frac{1}{2} \frac{e}{m_e} E_w \, (\pi/\omega_{ce})^2 \cos\psi < l_e = E_w \sin\psi \, / (B\omega_{ce}) \qquad (4.9)$$

$$\psi > \psi_r = \text{arc tg } \pi^2/2 = 79°$$

where $E_w = E(x_w)$. These electrons therefore hit the wall again and again and are finally absorbed. Therefore, for angles $\psi > \psi_r$ the sheath potential should become independent on γ_{re}. Another limit is reached if the reemission coefficient γ_{re} is increased above a critical value /13/ which is about 0.8 nearly independent on ψ. This is shown in Fig. 12. For increasing values of γ_{re} the electric field at the wall E_w decreases until, at the critical value of γ_{re}, $E_w = 0$. For even larger values of γ_{re}, the electric field E_w becomes instationary and temporarily negative. During the negative field periods electrons are driven back to the wall, so that in the mean no more electrons can escape the wall than at the critical value of γ_{re}.

Figure 13 shows profiles of density n, flow velocity $\underline{V}$, particle flux $\underline{\Gamma}$, temperature T_e, heat flux $\underline{Q}$, and electric potential ϕ across the sheath for a magnetic field angle $\psi = 85°$. For comparison with the case of perpendicular field incidence (Fig. 5), we have assumed equal particle and energy influx in both cases, i.e. the normal components of particle and energy flux Γ_x and Q_x at the sheath edge x_s are the same (the total fluxes at x_s along B then are larger for the oblique case by a factor $1/\cos\psi$). Since the dimension of the sheath in general is small compared to the mean free path for ionization (Fig. 3), we neglect particle and energy production in the sheath. Thus in a stationary 1d sheath

$$Z \, \Gamma_{ix} = \Gamma_{ex} = \Gamma_x = \text{const} \qquad (4.10)$$

and

$$S_{qi} = S_{qe} = 0.$$

Within the sheath preferentially the ion flux is turned from the B parallel direction towards the wall normal along x and twisted to some extent into the y direction. So a wall parallel current mainly along the z-direction arises in the sheath.

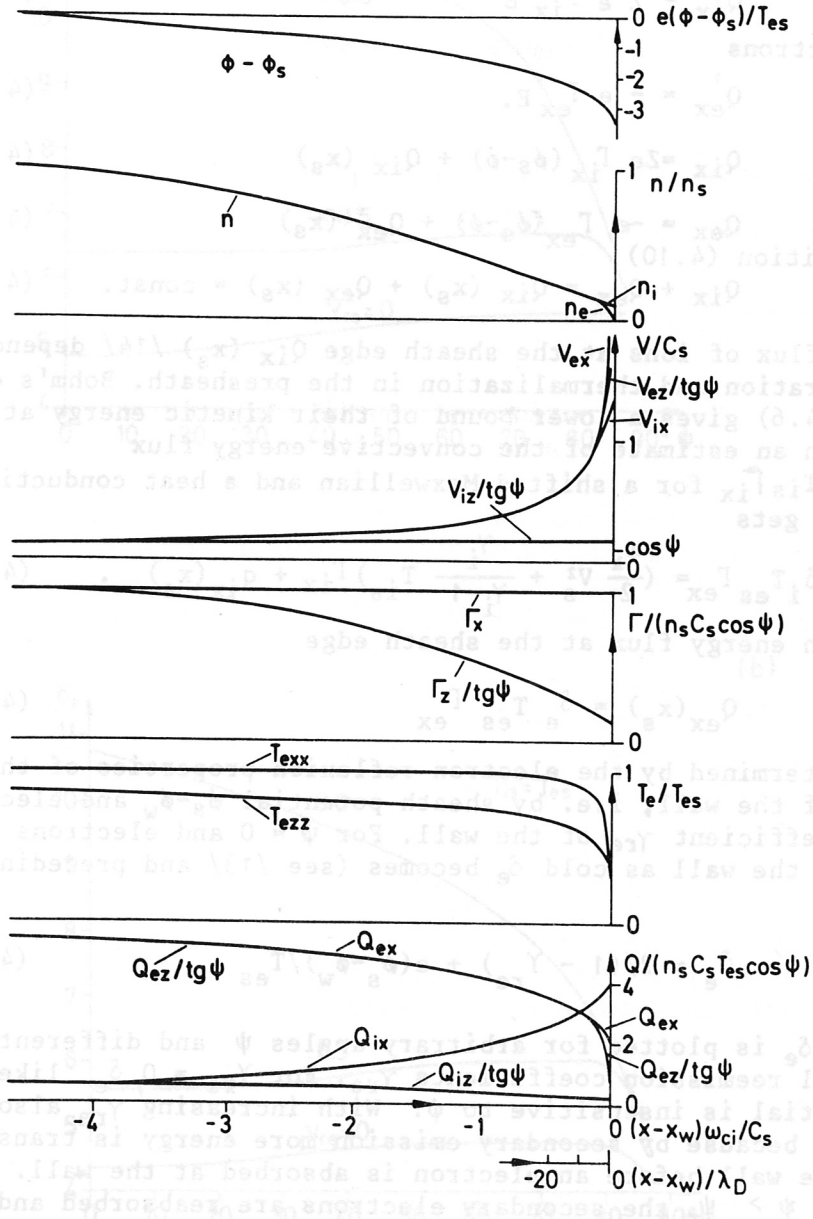

Fig. 13. Potential and flow variables in a sheath with oblique magnetic field. $\alpha = 1$, $\psi = 85°$, $T_{is} = 0$, $\gamma_{re} = 0$.

Also the energy flux of the ions is bent more strongly to the wall normal than that of the electrons. Ions gain energy flux in x direction (see eq. (3.6), ' = d/dx),

$$Q'_{ix} = Z\, e\, \Gamma_{ix}\, E \tag{4.11}$$

from the electrons

$$Q'_{ex} = -\, e\, \Gamma_{ex}\, E. \tag{4.12}$$

So

$$Q_{ix} = Ze\, \Gamma_{ix}(\phi_s - \phi) + Q_{ix}(x_s) \tag{4.13}$$

$$Q_{ex} = -e\, \Gamma_{ex}(\phi_s - \phi) + Q_{ex}(x_s) \tag{4.14}$$

and for condition (4.10)

$$Q_{ix} + Q_{ex} = Q_{ix}(x_s) + Q_{ex}(x_s) = \text{const.} \tag{4.15}$$

Energy flux of ions at the sheath edge $Q_{ix}(x_s)$ /14/ depends on their acceleration and thermalization in the presheath. Bohm's condition eq. (4.6) gives a lower bound of their kinetic energy at x_s. Together with an estimate of the convective energy flux $\gamma_i/(\gamma_i-1)\, T_{is}\Gamma_{ix}$ for a shifted Maxwellian and a heat conduction flux q_{ix} one gets

$$Q_{ix}(x_s) = \delta_i T_{es}\, \Gamma_{ex} = \left(\frac{m_i}{2} v_s^2 + \frac{\gamma_i}{\gamma_i - 1} T_{is}\right) \Gamma_{ix} + q_{ix}(x_s) \quad . \tag{4.16}$$

Electron energy flux at the sheath edge

$$Q_{ex}(x_s) = \delta_e\, T_{es}\, \Gamma_{ex} \tag{4.17}$$

is mainly determined by the electron reflexion properties of the sheath and of the wall, i.e. by sheath potential $\phi_s - \phi_w$ and electron reflexion coefficient γ_{re} of the wall. For $\psi = 0$ and electrons reflected from the wall as cold δ_e becomes (see /13/ and preceding Chapter)

$$\delta_e = 2/(1 - \gamma_{re}) + e(\phi_s - \phi_w)/T_{es} \quad . \tag{4.18}$$

In Fig. 14 δ_e is plotted for arbitrary angles ψ and different electron wall reemission coefficients γ_{re}. For $\gamma_{re} = 0$, δ_e like the sheath potential is insensitive to ψ. With increasing γ_{re} also δ_e is increased because by secondary emission more energy is transported to the wall before an electron is absorbed at the wall. For large angles $\psi > \psi_r$ the secondary electrons are reabsorbed and δ_e approaches the value for $\gamma_{re} = 0$.

From eqs. (4.13) and (4.14) together with (4.16) to (4.17), (4.10) and the results of Fig. 10 and Fig. 14 one gets the energy fluxes of

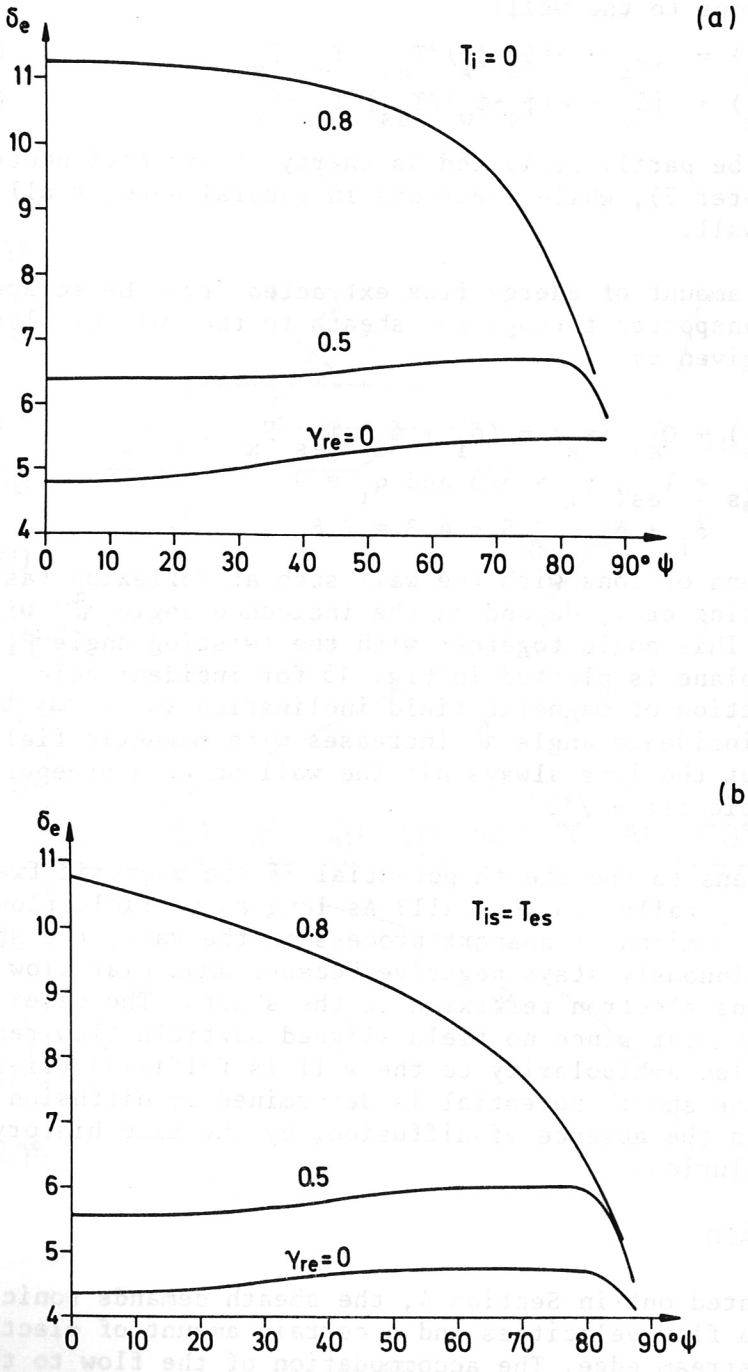

Fig. 14. Electron energy flux at the sheath edge per electron absorbed at the wall for different field angles ψ and secondary electron emission coefficient γ_{re}; a) $T_{is} = 0$, b) $T_{is} = T_{es}$.

ions and electrons to the wall:

$$Q_{ix}(x_w) = [\delta_i + e(\phi_s-\phi_w)/T_{es}]\, T_{es}\, \Gamma_x \qquad (4.19)$$

$$Q_{ex}(x_w) = [\delta_e - e(\phi_s-\phi_w)/T_{es}]\, T_{es}\, \Gamma_x . \qquad (4.20)$$

Ion energy may be partly reflected as energy of recycled neutral atoms (see Chapter 7), while electrons in general deposit all their energy at the wall.

The total amount of energy flux extracted from the scrape-off plasmas and transported through the sheath to the wall by plasma particles, is given by

$$Q_{ix}(x_s) + Q_{ex}(x_s) = (\delta_i + \delta_e)\, T_{es}\, \Gamma_x \quad . \qquad (4.21)$$

For $\gamma_{re} = 0$, $T_{is} = T_{es}$, $\gamma_i = 5/3$ and $q_i = 0$

$$\delta_i + \delta_e \cong 3.5 + 4.3 = 7.8 \quad .$$

Interactions of ions with the wall such as reflexion (as neutrals), sputtering etc., depend on the incidence angle ϑ_i with the wall normal x. This angle together with the twisting angle φ_i out of the ($\underline{E}$, $\underline{B}$)-plane is plotted in Fig. 15 for incident cold H^+-ions as function of magnetic field inclination ψ. As may be seen, the ion incidence angle ϑ_i increases with magnetic field inclination ψ but the ions always hit the wall under a steeper angle than the magnetic field /15/.

What happens to the sheath potential if the magnetic field becomes nearly parallel to the wall? As long as particle flow along B is the dominant transport process to the wall, the sheath potential continuously stays negative because ambipolar flow to the wall demands electron reflexion in the sheath. The case $\psi = 90°$ is singular since no field aligned particle flow reaches the wall and flow ambipolarity to the wall is fulfilled trivially. In this case the sheath potential is determined by diffusion flux across B or, in the absence of diffusion, by the time history of the sheath evolution.

5. THE PRESHEATH

As was pointed out in Section 4, the sheath demands sonic or supersonic plasma flow velocities and a certain amount of electron heat flux at its upstream edge. The accommodation of the flow to these conditions occurs in the so-called presheath region upstream of the sheath. Particle flow in the presheath originates from particles diffusing into the presheath from the main plasma and from ionization processes within the presheath. Energy is fed into the presheath from the core plasma by convection of the diffusing hot particles, and by heat conduction. In contrast to the sheath

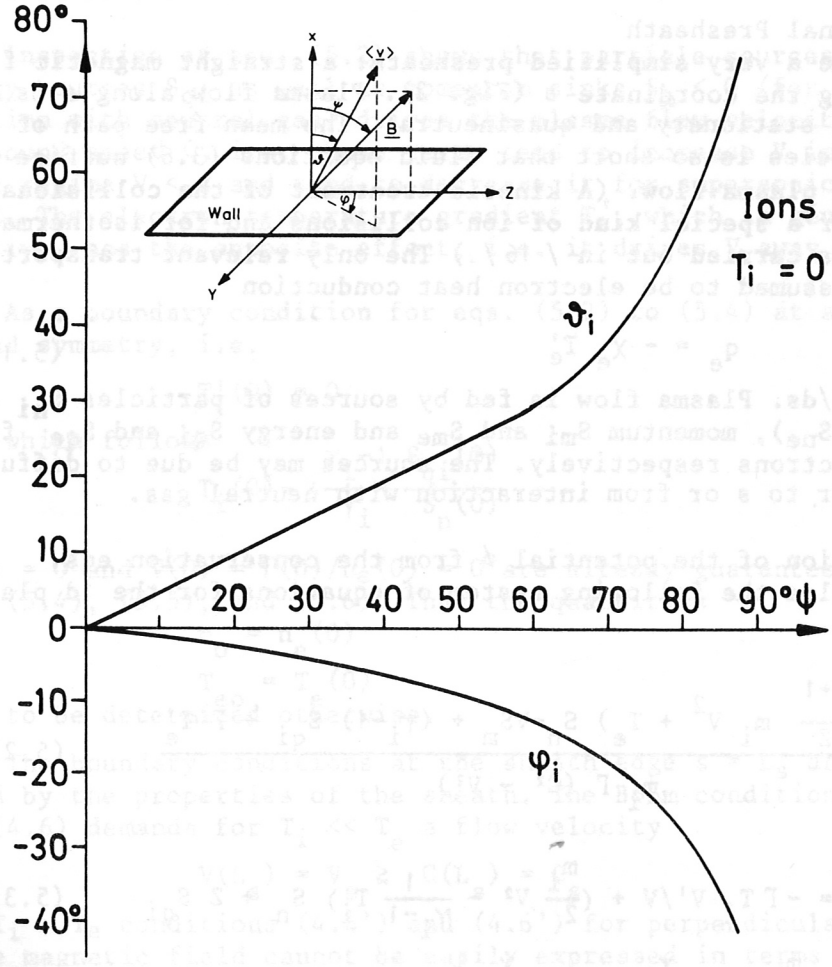

Fig. 15. Incidence angles (ϑ_i, φ_i) of cold ions at the wall for different field angles ψ ($\alpha = 1$, $\gamma_{re} = 0$).

the presheath in general is collisonal. Therefore collisional transport and relaxation within the flow has to be taken into account. In addition, the presheath comprises a large amount of interaction between plasma and neutral gas or impurities. These processes will be discussed in detail in Chapters 6 and 10 to 14. In this Section only some general features of the plasma flow in the presheath will be presented.

a) Collisional Presheath

Let us assume a very simplified presheath: a straight magnetic field extends along the coordinate s (Fig. 2). Plasma flow along s is one-dimensional, stationary and quasineutral. The mean free path of plasma particles is so short that fluid equations (3.6) suffice to describe the plasma flow. (A kinetic treatment of the collisional presheath for a special kind of ion collisions and for isothermal electrons was carried out in / 16 /.) The only relevant transport process is assumed to be electron heat conduction

$$q_e = - \chi_e T_e' \tag{5.1}$$

where $' = d/ds$. Plasma flow is fed by sources of particles S_{ni} and S_{ne} ($ZS_{ni} = S_{ne}$), momentum S_{mi} and S_{me} and energy S_{qi} and S_{qe} for ions and electrons respectively. The sources may be due to diffusion perpendicular to s or from interaction with neutral gas.

Elimination of the potential ϕ from the conservation eqs. (3.6) yields the following system of equations for the 1d plasma flow:

$$\frac{V'}{V} = Z \frac{(\frac{\gamma_i+1}{2Z} m_i V^2 + T_e) S_n - V S_m + (\gamma_i - 1) S_{qi} + \Gamma T_e'}{m_i \Gamma (C^2 - V^2)} \tag{5.2}$$

$$\frac{1}{\gamma_i - 1} \Gamma T_i' = - \Gamma T_i V'/V + (\frac{m_i}{2} V^2 - \frac{1}{\gamma_i - 1} T_i) S_n + Z S_{qi} \tag{5.3}$$

$$\chi_e T_e' = \Gamma (\frac{m_i}{2} V^2 + \frac{\gamma_i}{\gamma_i - 1} T_i + \frac{\gamma_e Z}{\gamma_e - 1} T_e)/Z - Q. \tag{5.4}$$

$S_n = ZS_{ni} = S_{ne}$, $S_m = S_{mi} + S_{me}$, S_{qi} and S_{qe} are the amounts of supplied particles, total momentum and energies to ions and electrons per length ds. Accordingly, the particle flux

$$\Gamma = \int_o^s S_n \, ds \tag{5.5}$$

and the total energy flux

$$Q = Q_i + Q_e = \int_o^s (S_{qi} + S_{qe}) \, ds.$$

are the accumulated particle and energy supplies. V is the common flow velocity of ions and electrons, $n_i = \Gamma/(ZV)$ and $n_e = \Gamma/V$ their densities, γ the ratio of specific heats, and

$$C^2 = (\gamma_i T_i + Z T_e)/m_i \tag{5.7}$$

the square of the sound speed C. (This specific form of the sound speed results from the assumptions of adiabatic ions and non-adiabatic electrons).

Inspection of equ. (5.2) shows that particle sources S_n and ion energy sources S_{qi} as well as momentum sinks $S_m < 0$ (for instance by friction with neutral gas) drives the plasma flow velocity towards the sound speed C, i.e. these terms tend to increase V in the subsonic regime $V < C$ and tend to decrease it for supersonic velocities $V > C$. The electron temperature gradient T_e', which in general is negative, has the opposite effect, i.e. it drives V away from C.

As a boundary condition for eqs. (5.2) to (5.4) at s = 0, we demand symmetry, i.e.

$$T_i'(0) = 0 \tag{5.8}$$

from which follows

$$T_i(0) = Z \frac{\gamma_i - 1}{\gamma_i} \frac{S_{qi}(0)}{S_n(0)} .$$

$T_e'(0) = 0$ and $V(0) = \Gamma(0)/n_e(0) = 0$ are already guaranteed by eqs. (5.4), (5.5), and (5.6). Thus the quantities

$$n_o = n_e(0)$$

and

$$T_{eo} = T_e(0)$$

have to be determined otherwise.

The boundary conditions at the sheath edge $s = L_s$ are determined by the properties of the sheath. The Bohm condition (4.4) and (4.6) demands for $T_i \ll T_e$ a flow velocity

$$V(L_s) = V_s \geq C(L_s) = C_s \tag{5.9}$$

(for $T_i \cong T_e$ conditions (4.4') and (4.6') for perpendicular or oblique magnetic field cannot be easily expressed in terms of low moments). Equation (4.17) together with the values for δ_e from Fig. 14 determines the electron energy flux

$$Q_e(L_s) = \frac{\gamma_e}{\gamma_e - 1} T_{es} \Gamma - \chi_{es} T_{es}' = \delta_e T_{es} \Gamma$$

The latter equation gives

$$T_{es}'/T_{es} = - [\delta_e - \gamma_e/(\gamma_e - 1)] \Gamma/\chi_{es} \tag{5.10}$$

The two free parameters n_o and T_{eo} must be chosen in such a way that conditions (5.9) and (5.10) are satisfied. Two cases are possible:

1) V is subsonic, $V < C$, in the whole presheath $0 \leq s \leq L_s$. Then V approaches C at the sheath edge, $V_s = C_s$. This boundary condition together with (5.10) determines n_o and T_{eo}.

2) V passes the sound speed C and becomes supersonic at the sheath edge, $V_s > C_s$. In this case, at the transition of V through C the numerator together with the denominator of the r.h.s. expression of eq. (5.2) must become zero, in order to keep V' finite. This condition together with the boundary condition (5.10)again determine

Which one of the two possibilities, 1) or 2), will be realized, depends on the distribution of the sources S and on the heat conductivity χ_e.

To illustrate the two different flow patterns 1) and 2), we assume two different particle sources: in case 1), particle Source S increases toward the wall, as it would be the case for ionization of neutrals recycled back from the wall,

$$S_n = \Gamma_1/d \exp [(s-L_s)/d]. \qquad (5.11)$$

In the other case, the particle source is located near the point x = 0, i.e. the particle source is remote from the wall,

$$S_n = \Gamma_1/d \exp (-s/d). \qquad (5.12)$$

It is assumed further that $S_m = S_{qi} = 0$ and χ_e = const for simplicity.

Figure 16a,b shows the solutions of system (5.2) to (5.4) under the boundary conditions (5.9) and (5.10) for these two cases. It depends on the size of the ratio $\sigma = \Gamma^2/(S_n \chi_e)$ whether or not V passes through the sound speed C. In case 1) σ is bounded, $\sigma = \Gamma d/\chi_e < 2$. The flow velocity rises at scale length d of the extension of the source to sound speed C and does not exceed it. In case 2) σ grows unlimitedly. The flow velocity first grows to sound speed at scale length d and proceeds to grow further at a scale length Γ/χ_e determined by the heat conductivity.

b) Collisionless Presheath

Let us now consider the other limiting case, where ions and electrons can run through the presheath without collisions after they entered the presheath by ionization or perpendicular diffusion. This kinetic problem has been treated analytically by many authors for different starting conditions of the ions and for isothermal electrons, /6, 9, 17/. By using the particle model described in Sect. 3, one can simulate the presheath without making assumptions on the electron distribution. Ions are assumed to start without energy,

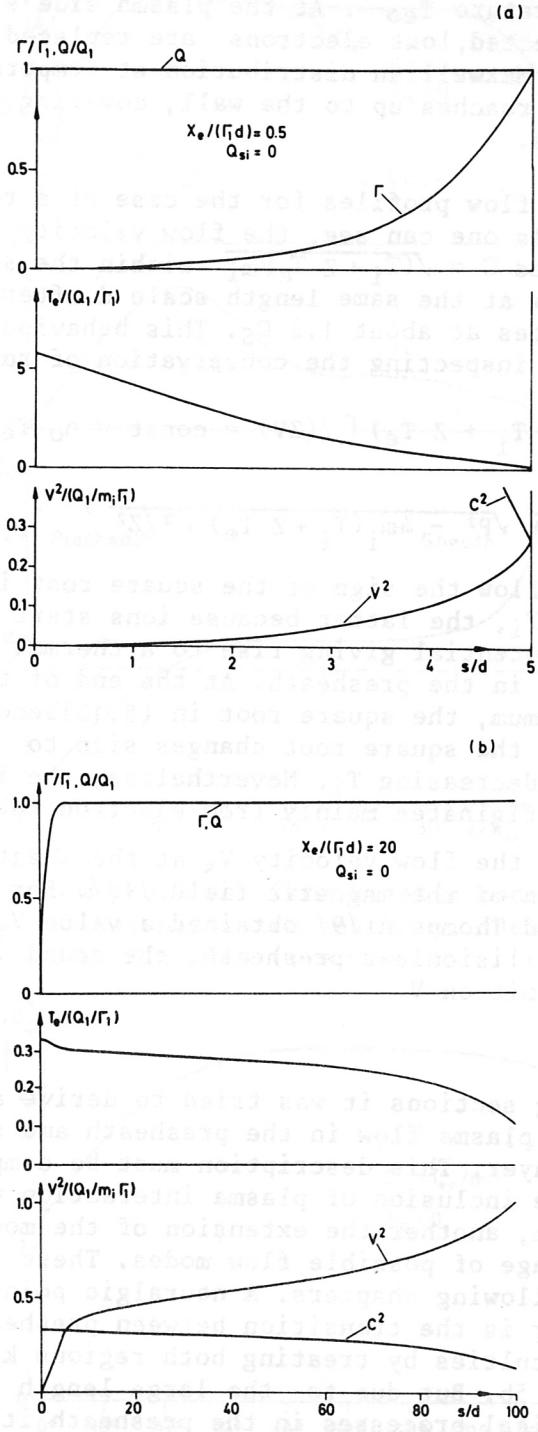

Fig. 16. Flow profiles in the presheath (from fluid equations) for different locations of the source;
a) $S_n = \Gamma_1/d \exp[(s - L_s)/d]$,
b) $S_n = \Gamma_1/d \exp(-s/d)$.

electrons with temperature T_{eo} . At the plasma side s = 0 ions are specularily reflected, lost electrons are replaced by the same number entering with Maxwellian distribution at temperature T_{eo}. The calculation area reaches up to the wall, covering the presheath as well as the sheath.

Figure 17 shows flow profiles for the case of a remote source given by eq. (5.12). As one can see, the flow velocity V grows up to isothermal sound speed $C = \sqrt{(T_i + Z\,T_e)/m_i}$ within the source region and continues to grow at the same length scale d after the source has ceased. V saturates at about 1.2 C_S. This behaviour of V can be better understood by inspecting the conservation of total momentum flow P

$$P = (m_i\,V^2 + T_i + Z\,T_e)\,\Gamma/(ZV) = \text{const} = n_o\,T_{eo} \quad .$$

Solving for V yields

$$V = \frac{Z}{2m_i\Gamma}\left(P \mp \sqrt{P^2 - 4m_i(T_i + Z\,T_e)\,\Gamma^2/Z^2}\right) \quad . \qquad (5.13)$$

At the start of the flow the sign of the square root is negative. Γ rises as well as T_i, the latter because ions start at different values of electric potential giving rise to a thermal spread of velocities. $T_e \cong T_{eo}$ in the presheath. At the end of the source region, T_i has a maximum, the square root in (5.13) becomes zero and $V = C_s$. For larger s the square root changes sign to + and V continues to rise with decreasing T_i. Nevertheless, the increase of ion kinetic energy originates mainly from electron thermal energy.

Figure 18 shows the flow velocity V_s at the sheath edge for different orientation of the magnetic field /18/. For $\psi = 0$ and $S_n \propto n^{\nu}$ Harrison and Thompson /9/ obtained a value $V_s/C_s = 1.144$. Thus, also in the collisionless presheath, the sound velocity is not necessarily a limit on V.

6. CONCLUSION

In the preceding sections it was tried to derive a coherent description of the 1d plasma flow in the presheath and sheath regions of the scrape-off layer. This description must be completed in many respects. One is the inclusion of plasma interaction with neutral gas in the presheath, another the extension of the models to 2d, which widens the range of possible flow modes. These topics will be discussed in the following chapters. A neuralgic point for modelling the scrape-off layer is the transition between presheath and sheath. One can avoid difficulties by treating both regions kinetically as was done in Section 5b. But due to the large length scale and the large number of physical processes in the presheath it is much more advantageous to treat this region on a fluid base. This leads to the problem that kinetic boundary conditions for the sheath must be derived from the fluid solution of the presheath and vice versa boundary conditions for the presheath from the kinetic solutions of the sheath. In order to solve this matching problem satisfactorily,

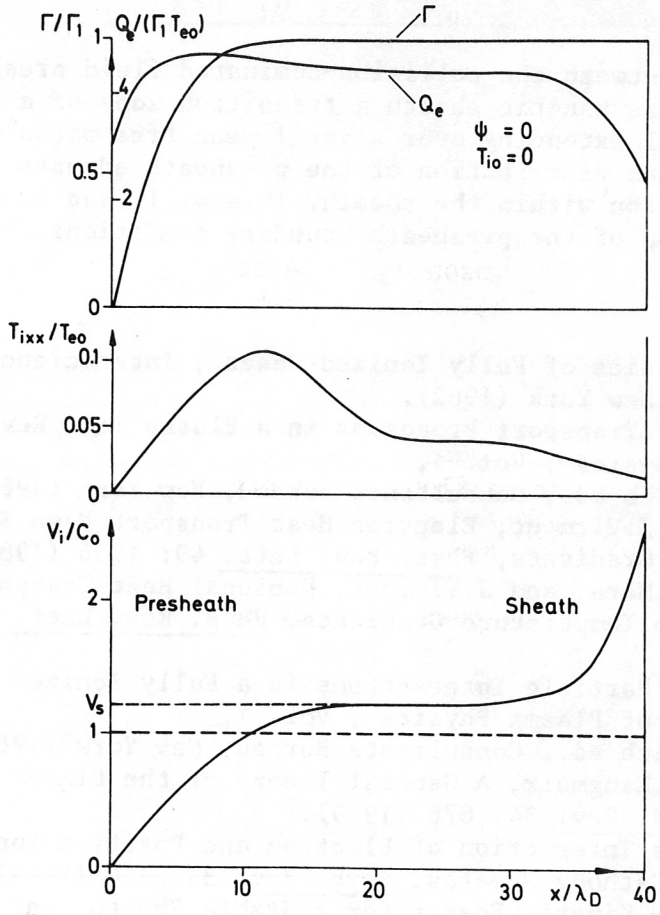

Fig. 17. Flow profiles (from kinetic model) in a collisionless presheath and sheath with S_n as in Fig. 16b ($\psi = 0$).

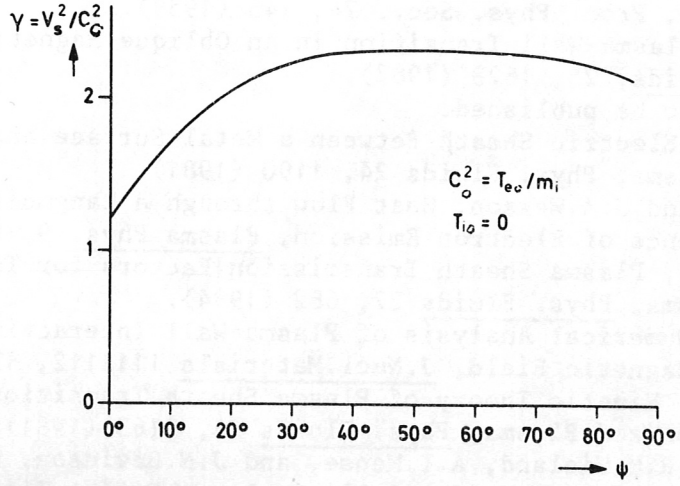

Fig. 18. Flow velocity at sheath edge V_S for a collisionless presheath as shown in Fig. 17 but for different field orientations ψ.

one has to put in between the collision-dominated fluid presheath and the collisionless kinetic sheath a transition zone of a collisional kinetic model extending over several mean free paths where the nearly Maxwellian distribution of the presheath adjusts to the truncated distribution within the sheath. This will lead to a more adequate formulation of the presheath boundary conditions.

References

/1/ L.Spitzer, Physics of Fully Ionized Gases , Interscience Publishers, New York (1962).

/2/ S.I.Braginskii, Transport Processes in a Plasma in: Review of Plasma Physics , Vol. 1, M.A.Leontovich ed., Consultants Bureau, New York (1965).

/3/ J.P.Matte, and J.Virmont, Electron Heat Transport Down Steep Temperature Gradients, Phys. Rev. Lett. 49: 1936 (1982).

/4/ J.F.Luciani, P.Mora, and J.Virmont, Nonlocal Heat Transport Due to Steep Temperature Gradients, Phys. Rev. Lett. 51: 1664 (1983).

/5/ B.A.Trubnikov, Particle Interactions in a Fully Ionized Plasma, in: Review of Plasma Physics , Vol. 1, M.A.Leontovich ed., Consultants Bureau, New York (1965).

/6/ L.Tonks, and I.Langmuir, A General Theory of the Plasma of an Arc, Phys. Rev. 34: 876 (1929).

/7/ I.Langmuir, The Interaction of Electron and Positive Ion Space Charges in Cathode Sheaths, Phys. Rev. 33: 954 (1929).

/8/ D.Bohm, Minimum Kinetic Energy for a Stable Sheath, in: The Characteristics of Electrical Discharges in Magnetic Fields , A.Guthrie, and R.K.Wakerling eds., McGraw Hill, New York (1949).

/9/ E.R.Harrison, and W.B.Thompson, The Low Pressure Plane Symmetric Discharge, Proc. Phys. Soc., 74, 145 (1959).

/10/ R.Chodura, Plasma-Wall Transition in an Oblique Magnetic Field, Phys. Fluids, 25, 1628 (1982).

/11/ R.Chodura, to be published.

/12/ U.Daybelge, Electric Sheath Between a Metal Surface and a Magnetized Plasma, Phys. Fluids 24, 1190 (1981).

/13/ G.D.Hobbs, and J.A.Wesson, Heat Flow through a Langmuir Sheath in the Presence of Electron Emission, Plasma Phys. 9, 85 (1967).

/14/ P.C.Stangeby, Plasma Sheath Transmission Factors for Tokamak Edge Plasma, Phys. Fluids 27, 682 (1984).

/15/ R.Chodura, Numerical Analysis of Plasma-Wall Interaction for an Oblique Magnetic Field, J.Nucl.Materials 111&112, 420 (1982).

/16/ K.U.Riemann, Kinetic Theory of Plasma Sheath Transition in a Weakly Ionized Plasma, Phys. Fluids 24, 2163 (1981).

/17/ G.A.Emmert, R.M.Wieland, A.T.Mense, and J.N.Davidson, Electric Sheath and Presheath in a Collisionless, Finite Ion Temperature Plasma, Phys. Fluids 23, 803 (1980).

/18/ R.Chodura, Plasma Transport to the Wall Through the Electrostatic Sheath, Proc. 11th Europ. Conf. on Controlled Fusion and Plasma Physics, Vol. 2, 479 (1983).